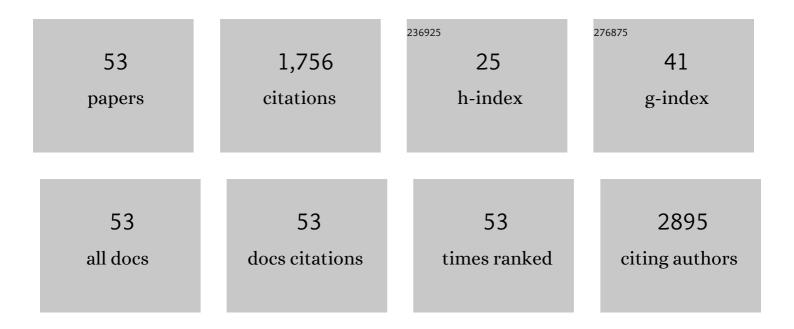
## Imtisal Akhtar

List of Publications by Year in descending order

Source: https://exaly.com/author-pdf/2375450/publications.pdf Version: 2024-02-01



Ινατιςλί Δκητλά

#	Article	IF	CITATIONS
1	High-mobility and air-stable single-layer WS2 field-effect transistors sandwiched between chemical vapor deposition-grown hexagonal BN films. Scientific Reports, 2015, 5, 10699.	3.3	258
2	Atomic force microscopy and spectroscopy. Reports on Progress in Physics, 2008, 71, 016101.	20.1	118
3	Influence of an Al2O3 interlayer in a directly grown graphene-silicon Schottky junction solar cell. Carbon, 2018, 132, 157-164.	10.3	78
4	n-MoS <sub>2</sub> /p-Si Solar Cells with Al <sub>2</sub> O <sub>3</sub> Passivation for Enhanced Photogeneration. ACS Applied Materials & Interfaces, 2016, 8, 29383-29390.	8.0	77
5	Synthesis and characterization of large-area and continuous MoS <sub>2</sub> atomic layers by RF magnetron sputtering. Nanoscale, 2016, 8, 4340-4347.	5.6	74
6	Influence of removing PMMA residues on surface of CVD graphene using a contact-mode atomic force microscope. RSC Advances, 2017, 7, 6943-6949.	3.6	68
7	Enhanced photoresponse of ZnO quantum dot-decorated MoS <sub>2</sub> thin films. RSC Advances, 2017, 7, 16890-16900.	3.6	59
8	Supercapacitors based on Ti3C2Tx MXene extracted from supernatant and current collectors passivated by CVD-graphene. Scientific Reports, 2021, 11, 649.	3.3	54
9	Thickness-dependent efficiency of directly grown graphene based solar cells. Carbon, 2019, 148, 187-195.	10.3	49
10	Multifunctional and high-performance GeSe/PdSe <sub>2</sub> heterostructure device with a fast photoresponse. Journal of Materials Chemistry C, 2020, 8, 4743-4753.	5.5	47
11	Micro-to-nano-scale deformation mechanisms of a bimodal ultrafine eutectic composite. Scientific Reports, 2014, 4, 6500.	3.3	46
12	Polymer-dispersed liquid-crystal-based switchable glazing fabricated <i>via</i> vacuum glass coupling. RSC Advances, 2020, 10, 32225-32231.	3.6	41
13	Asymmetric electrode incorporated 2D GeSe for self-biased and efficient photodetection. Scientific Reports, 2020, 10, 9374.	3.3	38
14	Application of Titanium-Carbide MXene-Based Transparent Conducting Electrodes in Flexible Smart Windows. ACS Applied Materials & Interfaces, 2021, 13, 40976-40985.	8.0	37
15	Acrylate-assisted fractal nanostructured polymer dispersed liquid crystal droplet based vibrant colored smart-windows. RSC Advances, 2019, 9, 12645-12655.	3.6	36
16	High mobility ReSe <sub>2</sub> field effect transistors: Schottky-barrier-height-dependent photoresponsivity and broadband light detection with Co decoration. 2D Materials, 2020, 7, 015010.	4.4	36
17	Effect of Annealing in Ar/H <sub>2</sub> Environment on Chemical Vapor Deposition-Grown Graphene Transferred With Poly (Methyl Methacrylate). IEEE Nanotechnology Magazine, 2015, 14, 70-74.	2.0	34
18	WSe <sub>2</sub> Homojunction p–n Diode Formed by Photoinduced Activation of Mid-Gap Defect States in Boron Nitride. ACS Applied Materials & Interfaces, 2020, 12, 42007-42015.	8.0	34

IMTISAL AKHTAR

#	Article	IF	CITATIONS
19	NIR self-powered photodetection and gate tunable rectification behavior in 2D GeSe/MoSe2 heterojunction diode. Scientific Reports, 2021, 11, 3688.	3.3	34
20	Low-temperature high-resolution magnetic force microscopy using a quartz tuning fork. Applied Physics Letters, 2005, 87, 103103.	3.3	31
21	Highly aligned carbon nanotubes and their sensor applications. Nanoscale, 2020, 12, 21447-21458.	5.6	31
22	Ultravioletâ€Lightâ€Induced Reversible and Stable Carrier Modulation in MoS <sub>2</sub> Fieldâ€Effect Transistors. Advanced Functional Materials, 2014, 24, 7125-7132.	14.9	30
23	Combinatorial Influence of Bimodal Size of B2 TiCu Compounds on Plasticity of Ti-Cu-Ni-Zr-Sn-Si Bulk Metallic Glass Composites. Metallurgical and Materials Transactions A: Physical Metallurgy and Materials Science, 2014, 45, 2376-2381.	2.2	27
24	High performance complementary WS <sub>2</sub> devices with hybrid Gr/Ni contacts. Nanoscale, 2020, 12, 21280-21290.	5.6	27
25	Optoelectronics of Multijunction Heterostructures of Transition Metal Dichalcogenides. Nano Letters, 2020, 20, 1934-1943.	9.1	27
26	Self-standing SnS nanosheet array: a bifunctional binder-free thin film catalyst for electrochemical hydrogen generation and wastewater treatment. Dalton Transactions, 2021, 50, 12723-12729.	3.3	27
27	Effect of Ti <sub>3</sub> C <sub>2</sub> T <sub>x</sub> MXenes etched at elevated temperatures using concentrated acid on binder-free supercapacitors. RSC Advances, 2020, 10, 41837-41845.	3.6	26
28	Study of Grains and Boundaries of Molybdenum Diselenide and Tungsten Diselenide Using Liquid Crystal. Nano Letters, 2017, 17, 1474-1481.	9.1	24
29	Solar cell based on vertical graphene nano hills directly grown on silicon. Carbon, 2020, 164, 235-243.	10.3	23
30	Gate Tunable Transport in Graphene/MoS2/(Cr/Au) Vertical Field-Effect Transistors. Nanomaterials, 2018, 8, 14.	4.1	22
31	Van der Waals heterojunction diode composed of WS <sub>2</sub> flake placed on p-type Si substrate. Nanotechnology, 2018, 29, 045201.	2.6	21
32	Effect of the Photoinitiator Concentration on the Electro-optical Properties of Thiol–Acrylate-Based PDLC Smart Windows. ACS Applied Energy Materials, 2022, 5, 6986-6995.	5.1	21
33	Gate Modulation of the Spin-orbit Interaction in Bilayer Graphene Encapsulated by WS2 films. Scientific Reports, 2018, 8, 3412.	3.3	20
34	A facile route to a high-quality graphene/MoS <sub>2</sub> vertical field-effect transistor with gate-modulated photocurrent response. Journal of Materials Chemistry C, 2017, 5, 2337-2343.	5.5	19
35	Twist-Angle-Dependent Optoelectronics in a Few-Layer Transition-Metal Dichalcogenide Heterostructure. ACS Applied Materials & Interfaces, 2019, 11, 2470-2478.	8.0	19
36	Real-time atomic force microscopy using mechanical resonator type scanner. Review of Scientific Instruments, 2008, 79, 103703.	1.3	16

IMTISAL AKHTAR

#	Article	IF	CITATIONS
37	Operation Protocols To Improve Durability of Protonic Ceramic Fuel Cells. ACS Applied Materials & Interfaces, 2019, 11, 457-468.	8.0	14
38	Stretchable Sensor Made of MWCNT/ZnO Nanohybrid Particles in PDMS. Advanced Materials Technologies, 2020, 5, 2000229.	5.8	14
39	Studies on directly grown few layer graphene processed using tape-peeling method. Carbon, 2020, 158, 749-755.	10.3	12
40	Highâ€Efficiency Supercapacitor Electrodes of <scp>CVD</scp> â€grown Graphenes Hybridized with Multiwalled Carbon Nanotubes. Bulletin of the Korean Chemical Society, 2015, 36, 2111-2115.	1.9	11
41	Effect of additional HfO <sub>2</sub> layer deposition on heterojunction c‣i solar cells. Energy Science and Engineering, 2018, 6, 706-715.	4.0	10
42	Visualizing Degradation of Black Phosphorus Using Liquid Crystals. Scientific Reports, 2018, 8, 12966.	3.3	10
43	Radial alignment of carbon nanotubes for directional sensing application. Composites Part B: Engineering, 2021, 222, 109038.	12.0	10
44	Three-dimensional atomic force microscopy for ultra-high-aspect-ratio imaging. Applied Surface Science, 2019, 469, 582-592.	6.1	9
45	QUARTZ CRYSTAL RESONATOR BASED SCANNING PROBE MICROSCOPY. Modern Physics Letters B, 2005, 19, 1303-1322.	1.9	8
46	Mechanical properties of rippled structure in suspended stacks of graphene. Journal of Applied Physics, 2010, 108, .	2.5	7
47	Dynamics of liquid crystal on hexagonal lattice. 2D Materials, 2018, 5, 045021.	4.4	5
48	Modulation of Magnetoresistance Polarity in BLG/SL-MoSe2 Heterostacks. Nanoscale Research Letters, 2020, 15, 136.	5.7	4
49	Effect of Poly(2-ethyl-2-oxazoline) on Multi-Walled Carbon Nanotubes Reinforced Poly(vinyl alcohol) Composites. Polymers and Polymer Composites, 2010, 18, 251-256.	1.9	3
50	Nanographene device fabrication using atomic force microscope. Micro and Nano Letters, 2013, 8, 422-425.	1.3	3
51	Raman spectroscopic image analysis on micropatterned graphene. Micro and Nano Letters, 2013, 8, 362-365.	1.3	3
52	General algorithm and method for scanning a via hole by using critical-dimension atomic force microscopy. Journal of the Korean Physical Society, 2014, 64, 1643-1647.	0.7	3
53	Quartz tuning fork based three-dimensional topography imaging for sidewall with blind features. Ultramicroscopy, 2020, 210, 112916.	1.9	1